Journal of Algorithms and Computations

journal homepage: http://jac.ut.ac.ir

Mixed-Norm Inversion of Full-Tensor Gravity and Magnetic Data for High-Resolution Subsurface Imaging

F. Didar[1], M. Hosseini[1], M. Abedi[*1], V. Ebrahimzadeh Ardestani[2]

[1] Petroleum Engineering and Geophysics Laboratory, School of Mining Engineering, College of Engineering, University of Tehran, Iran.

[2] Institute of Geophysics, University of Tehran, Iran.

ABSTRACT

This study develops a unified framework for full-tensor gravity-gradient and full-tensor magnetic forward modelling and inversion using a mixed-norm regularization approach for subsurface physical property reconstruction. By utilizing all components of both gravity and magnetic gradient tensors, the forward modelling stage captures the full directional sensitivity of the potential fields, providing a more informative representation of subsurface structures than conventional approaches. The inversion is formulated as a constrained optimization problem and solved using a projected Gauss–Newton conjugate gradient method combined with an iterative reweighted least squares scheme. Mixed-norm ensures a balance between compactness and smoothness, enabling recovery of sharp interfaces and smooth background variations. Sensitivity-based weighting and physical property bounds enhance stability and robustness. Overall, the study highlights the effectiveness of full-tensor gravity and magnetic inversion for improved subsurface imaging.

Keywords: Full-tensor gravity gradient (FTG), Full-tensor magnetic gradient (FTM), Mixed-norm regularization, Forward modeling, Geophysical inversion

ARTICLE INFO

Article history:
Research paper
Received 11, May 2026
Accepted 08, June 2026
Available online 15, June 2026

AMS subject classification: 90C06

[†] Corresponding author: M. Abedi, Email: maysamabedi@ut.ac.ir.

1 Introduction

Potential field methods are among the most important and widely used geophysical tools for investigating subsurface structures of the Earth. Owing to their non-invasive nature, relatively low operational cost, wide spatial coverage, and applicability across multiple scales, these methods are extensively applied in mineral exploration, hydrocarbon studies, tectonic investigations, subsurface cavity detection, and engineering geology applications[1-3]. Among potential field techniques, gravity and magnetic data play a central role in imaging and interpreting Earth's interior due to their direct sensitivity to subsurface density and magnetization variations, respectively. Variations in the gravity and magnetic fields provide valuable information about physical property heterogeneities, geological structures, and lithological boundaries [3-5]. Compared to many other geophysical methods, both gravity and magnetic surveys are capable of probing deep structures and remain effective even in geologically complex environments. Furthermore, advances in high-precision instrumentation, together with developments in processing and numerical modeling techniques, have significantly improved the accuracy and resolution of potential field data in recent decades[6]. However, conventional gravity and magnetic data are often limited in resolving complex subsurface structures due to the inherent smoothness of potential fields and the associated non-uniqueness problem[5, 7, 8]. As a result, the use of gradient-based data, particularly full-tensor gravity and full-tensor magnetic data, has attracted considerable attention as an effective approach for enhancing resolution and extracting finer structural details from the subsurface [8-11].

Despite the widespread application of gravity and magnetic data in subsurface investigations, the interpretation of conventional potential-field measurements is associated with several fundamental challenges. Owing to the potential-field nature of gravity and magnetic anomalies, the observed responses generally exhibit smooth and low-frequency characteristics, causing signals from different subsurface sources to overlap and complicating the resolution of complex geological structures[1, 3, 5]. Furthermore, both gravity and magnetic inversion are inherently ill-posed and non-unique problems, meaning that different distributions of density and magnetization can generate similar observed responses[3, 5, 7, 12]. This non-uniqueness reduces spatial resolution and increases ambiguity in determining the geometry, depth, and physical properties of subsurface structures. In conventional surveys, only limited components of the gravity or magnetic field are typically measured, resulting in the loss of valuable directional information related to field variations. This limitation becomes particularly critical in geologically complex environments and in the investigation of shallow or small-scale targets, where conventional datasets often fail to accurately resolve structural boundaries and lateral variations[6, 10, 11]. Moreover, traditional gravity and magnetic data generally exhibit limited sensitivity to sharp physical property contrasts and structural edges, which further complicates accurate geological interpretation[١٣]. Consequently, gradient-based techniques, particularly full-tensor gravity and full-tensor magnetic methods, have emerged as powerful tools for enhancing spatial resolution and improving the characterization of subsurface structures.

To overcome these limitations, the use of gradient-based potential field data, particularly full tensor gravity (FTG) and full tensor magnetic (FTM) methods, has attracted considerable attention in recent decades. In these approaches, instead of measuring only the gravity or magnetic fields, their spatial derivatives are measured in the form of gradient tensors, providing more detailed information about subsurface density and magnetization variations [3, 5, 9-11, 13, 14]. The gravity

gradient tensor consists of multiple components, each of which exhibits different sensitivity to the geometry and orientation of geological structures. Therefore, the simultaneous use of all tensor components can enhance resolution, improve boundary detection, and reduce interpretational ambiguity [11, 15]. Both gravity and magnetic gradient tensors consist of multiple components, each exhibiting different sensitivity to the geometry, orientation, and physical properties of geological structures. Consequently, the simultaneous use of all tensor components can significantly enhance spatial resolution, improve boundary detection, and reduce interpretational ambiguity [10, 11, 16]. The development of high-precision FTG and FTM systems, particularly for airborne applications, has enabled higher-resolution imaging of subsurface structures and expanded the use of these techniques in mineral exploration, hydrocarbon studies, tectonic investigations, and characterization of complex geological environments[13, 14]. As a result, forward modelling and inversion of full-tensor gravity and magnetic data have become active and rapidly developing research areas in modern exploration geophysics.

Forward modeling is considered one of the fundamental components in geophysical studies based on potential-field methods and plays a key role in the development, evaluation, and validation of inversion techniques. In essence, forward modeling enables the computation of the theoretical response of a physical field (such as gravity or magnetics) from an assumed subsurface model and acts as a link between the geological model and the observed data [1, 4]. In exploration geophysics, the importance of forward modeling arises from the fact that data interpretation is often formulated as an inverse problem; however, before any inversion is performed, the relationship between model parameters and data must be accurately and stably defined. In this context, forward modeling serves as a primary tool for generating synthetic datasets, investigating the sensitivity of responses to variations in model parameters, and evaluating system behavior under different geological scenarios[2]. One of the key advantages of forward modeling is its ability to systematically examine the effect of geometry, density, and subsurface structural distribution on the observed field. This allows researchers to isolate and analyze the role of individual parameters, leading to a deeper understanding of the physical nature of the problem. In addition, forward modeling plays an important role in the optimal design of geophysical surveys and in assessing the resolution capability of measurement systems[6].

In modern geophysical methods, particularly in potential-field data analysis, forward modeling also serves as the foundation for the development of numerical inversion algorithms. Many iterative inversion schemes directly rely on a forward operator to compute model responses at each iteration; therefore, the accuracy, stability, and computational efficiency of forward modeling directly influence the quality of the final inversion results[5]. In recent years, with advances in numerical methods and increased computational power, forward modeling for complex three-dimensional geometries and multi-component datasets—including full tensor gravity data—has gained significant attention. In this regard, the use of detailed 3D models and efficient computational techniques such as volumetric discretization methods, numerical integration, and fast transforms has enabled more realistic simulations of physical fields [5, 9, 10]. Overall, forward modeling is not only a computational tool but also a conceptual framework for understanding the physical behavior of geophysical data, playing a fundamental role in linking geological models to real-world observations.

Inversion of geophysical data, particularly in potential-field methods such as gravity and magnetic surveys, is inherently associated with fundamental and computational challenges. The problem is intrinsically ill-posed, meaning that a unique solution does not exist and that multiple subsurface models can reproduce the same observed data[1, 7, 12, 17]. Together with the naturally smooth and diffusive behavior of both gravity and magnetic fields, this leads to a loss of both depth and lateral resolution in surface measurements, resulting in significant ambiguity in imaging complex subsurface structures. In addition to non-uniqueness, the inversion process is highly sensitive to data noise and is governed by an ill-conditioned forward operator, where even small perturbations in the data may cause large instabilities in the recovered model[3, 5, 18]. Furthermore, the limited depth sensitivity of both gravity and magnetic data increases uncertainty in resolving deep structures, requiring additional constraints to stabilize the inversion problem[5]. To address these challenges, regularization methods have become a standard approach in geophysical inversion. These methods incorporate prior information or mathematical constraints into the problem, thereby reducing the solution space and producing more stable and physically plausible models[19]. In classical formulations, ℓ_{pq} norms are commonly used to enforce smoothness or sparsity separately; however, neither approach alone is capable of simultaneously representing smooth variations and sharp geological discontinuities in complex subsurface environments. In this context, mixed-norm regularization has emerged as an effective strategy for improving inversion quality. This approach allows the combination of the advantages of different norms, enabling simultaneous control over model smoothness and the preservation of sharp geological boundaries. In other words, mixed-norm formulations produce inversion results that are both physically stable and more geologically realistic. Accordingly, in this study, a mixed-norm-based inversion framework is employed to enhance the stability and accuracy of subsurface reconstruction using full tensor gravity data[20, 21].

The main objective of this study is to develop and evaluate a mixed-norm-based inversion framework for full-tensor gravity and full-tensor magnetic data and to investigate the behavior of each tensor component in reconstructing subsurface structures. In this context, a three-dimensional forward modelling scheme is first implemented to compute full-tensor gravity and magnetic responses from an assumed subsurface model. Subsequently, a mixed-norm regularized inversion algorithm is applied to reconstruct the subsurface density and susceptibility distributions in a manner consistent with the observed data. The primary focus of this research is to analyze the sensitivity and contribution of each gravity and magnetic tensor component within the inversion process, and to assess their capability in resolving geological structures with different geometries and depths. In other words, this study aims to determine to what extent the integration of full-tensor gravity and magnetic components within a mixed-norm regularization framework can improve subsurface imaging quality and reduce inversion ambiguity compared to classical approaches.

Geophysical modeling was performed using the open-source SimPEG library (version 0.25.2), which provides a powerful tool for parameter estimation[22]. The inversion modeling was performed on a system consisting of an ASUS laptop equipped with an Intel® Core™ i7-13620H processor (base frequency 2.4 GHz) and 32 GB of RAM.

2 Methodology

In this section, we first present the mathematical formulation of gravity and magnetic forward modelling. Subsequently, a detailed description of the mixed-norm inversion framework is provided, focusing on the independent inversion of gravity data set.

2.1 Forward modelling

Solving the forward problem enables the prediction of geophysical data associated with specific subsurface geological structures. In essence, by using model parameters ($\mathbf{c}$) as an example, the corresponding data ($\mathbf{d}$) can be estimated through the forward modelling operator As, which links the observed response to the causative source $\boldsymbol{s}$ [23].

$$\boldsymbol{d} = A_{\boldsymbol{s}}(\boldsymbol{c}). \tag{1}$$

For full-tensor gravity gradient forward modelling, all components of the gravity gradient tensor are considered rather than a single vertical term. The observed response is related to the subsurface density distribution through the corresponding sensitivity kernels T_{ij}, which map the density contrast of each discretized cell (ρ) into the predicted gravity-gradient tensor response at the observation point P (x_P, y_P, z_P). In this framework, each tensor component g_{ij} is expressed as the integral effect of the subsurface density distribution weighted by its respective kernel, enabling a more complete and detailed representation of the subsurface structure[24].

$$\begin{bmatrix} g_{xx} \\ g_{xy} \\ g_{xz} \\ g_{yy} \\ g_{yz} \\ g_{zz} \end{bmatrix} = \begin{bmatrix} T_{xx} \\ T_{xy} \\ T_{xz} \\ T_{yy} \\ T_{yz} \\ T_{zz} \end{bmatrix} \rho \tag{2}$$

The full gravity gradient tensor is employed in this study rather than a single vertical component, due to its ability to capture the complete directional information of the gravitational field. Compared with conventional gravity data, the full tensor formulation provides enhanced sensitivity to both lateral and vertical variations in subsurface density, leading to improved spatial resolution and reduced ambiguity in structural interpretation. The forward response can be expressed in compact form as:

$$\boldsymbol{g} = \boldsymbol{T}\rho\ . \tag{3}$$

where $\boldsymbol{T}$ represents the full sensitivity tensor operator and ρ denotes the density contrast distribution.

The components of the full gravity gradient tensor T_{ij} are computed analytically using the rectangular prism formulation, which provides a closed-form solution for the gravitational response of a constant-density cell. In this framework, each tensor component is obtained by evaluating a corresponding kernel function over the boundaries of the discretized prism:

$$T_{ij} = \boldsymbol{G} \cdot \boldsymbol{F}_{ij}(x, y, z) \Big|_{x_L}^{x_U} \Big|_{y_L}^{y_U} \Big|_{z_L}^{z_U} . \quad (4)$$

where (x_L, y_L, z_L) and (x_U, y_U, z_U) denote the lower southwest and upper northeast corners of each rectangular prism, respectively. These geometric parameters are used to evaluate all kernel contributions required to construct the full gravity gradient tensor, thereby enabling a complete and consistent description of the subsurface density distribution. In addition, $\boldsymbol{F}_{ij}$ represents the analytical kernel associated with the second-order spatial derivatives of the gravitational potential, and $i, j \in \{x, y, z\}$. The term $\boldsymbol{G}$ denotes the universal gravitational constant, which scales the magnitude of the gravitational response and ensures the physical consistency of the modeled field . The relative position vector between the observation point $P(x_p, y_p, z_p)$ and an arbitrary point within the prism is defined as:

$$dx = (x_p - x), dy = (y_p - y), dz = (z_p - z). \quad (5)$$

and the Euclidean distance is given by:

$$r = \sqrt{({d_x}^2 + {d_y}^2 + {d_z}^2)} \quad (6)$$

In full-tensor gravity-gradient forward modelling, the observed responses are governed by the second-order spatial derivatives of the gravitational potential, providing significantly higher sensitivity to both lateral and vertical density variations compared with conventional gravity data (g_z). By simultaneously incorporating all independent tensor components, the FTG formulation enhances the resolution of small-scale geological features and reduces ambiguity in subsurface interpretation. For a large number of observation points, the forward problem can be expressed in compact matrix form as given in Eq. (7)[25].

$$\boldsymbol{g}^{pre} = \mathbf{F}_{\boldsymbol{G}} \rho \quad (7)$$

In Eq. (7), $\mathbf{F}_{\boldsymbol{G}}$ denotes the full-tensor gravity forward operator matrix, which maps the subsurface density model into the predicted data space, represented by $\boldsymbol{g}^{pre}$. The model parameter vector $\rho \in R^{\mathrm{M}}$ contains the density contrast values of all discretized cells, while the predicted data vector $\boldsymbol{g}^{pre} \in R^{\mathrm{N}}$ includes the calculated responses of the gravity gradient tensor at all observation locations. The forward operator matrix $\mathbf{F}_{\boldsymbol{G}} \in R^{\mathrm{N}\times\mathrm{M}}$ describes the sensitivity relationship between the density distribution and the observed tensor responses, where *M* represents the total number of model cells and *N* corresponds to the total number of FTG observations[23, 25].

For full-tensor magnetic forward modelling[26, 27], the forward problem is formulated in a manner analogous to the gravity case in Eq. (2). The relationship between the subsurface magnetization model and the observed data is expressed in Eq. (8). In this formulation, the model vector is defined as $\mathbf{m}^* = [M_x, M_y, M_z]^T$, representing the three components of magnetization within each discretized cell. The corresponding data vector consists of the full magnetic gradient tensor components, $\mathbf{b} = [b_{xx}, b_{xy}, b_{xz}, b_{yy}, b_{yz}, b_{zz}]^T$. The forward operator $\mathbf{S}$ represents the sensitivity (kernel) matrix that establishes a linear relationship between the magnetization distribution and the full-tensor magnetic responses at the observation points.

$$\mathbf{b} = \mathbf{S}\mathbf{m}^* . \quad (8)$$

The tensor **S**, as defined in Eq. (9), represents the magnetic gradient tensor, which is a symmetric, trace-free second-order tensor. Its components describe the spatial derivatives of the magnetic field and satisfy the symmetry conditions $S_{ij} = S_{ji}$, with zero trace $S_{xx} + S_{yy} + S_{zz} = 0$. The tensor can be expressed as:

$$\mathbf{S} = \frac{\mu_0}{4\pi}\begin{bmatrix} S_{xx} & S_{xy} & S_{xz} \\ S_{xy} & S_{yy} & S_{zy} \\ S_{xz} & S_{yz} & S_{zz} \end{bmatrix}. \quad (9)$$

where μ_0 denotes the magnetic permeability of free space, which acts as a scaling constant relating the magnetization source to the observed magnetic field gradients[26, 27].

Finally, we can formulate the magnetic forward modelling equation analogous to Eq. (7), as shown in Eq. (10). Here, $\mathbf{F_T}$ is the forward operator matrix for magnetic modelling, with $\mathbf{m}^* \in R^{3\mathrm{M}}$, $\mathbf{b}^{pre} \in R^{\mathrm{N}}$, $\mathbf{F_T} \in R^{\mathrm{N}\times 3\mathrm{M}}$ [26, 27].

$$\mathbf{b}^{pre} = \mathbf{F_T}\mathbf{m}^* . \quad (10)$$

2.2 Inverse modelling

The theoretical foundation for the inversion methodology employed within the SimPEG framework is laid out in the pioneering works of Li and Oldenberg (1998) [5].

$$min\phi(m) = \phi_d + \beta\phi_m . \quad (11)$$

In Eq. (8), $\phi(m)$ represents the objective function minimized during the inversion process. The data misfit term ϕ_d measures the agreement between the observed and predicted full-tensor gravity and full-tensor magnetic data, ensuring consistency between the recovered models and both datasets. The term ϕ_m denotes the regularization function, which imposes geological and mathematical constraints on the recovered density and susceptibility models to ensure physically plausible solutions. The regularization parameter β controls the trade-off between data fitting and model stability, balancing the contributions of the data misfit and regularization terms within the overall objective function[5].

Under the mixed-norm ℓ_{pq} framework[20, 21], the regularization term is formulated with $(0 \leq p, q \leq 2)$. This approach enhances model flexibility by allowing different norms to be applied to different components of the regularization term, leading to more accurate subsurface models and reduced exploration uncertainty and cost. The norm parameters are adjusted within the range of 0 to 2 to control model behavior. Specifically, $p_s = 0$ promotes compact models with sharp boundaries and improved target recovery, $p_s = 2$ yields smoother and more diffusive models with weaker boundary definition, and $p_s = 1$ provides an intermediate balance between these two extremes[20].

$$\phi_m^{pq} = \alpha_s \|\mathbf{W_s V_s R_s(m)}\|^p + \sum_{r=x,y,z} \alpha_r \|\mathbf{W_r V_r R_r D}_r\mathbf{(m)}\|^q \quad (12)$$

In Eq. (12), ϕ_m^{pq} defines the mixed-norm model regularization term used to control both the amplitude and spatial variability of the recovered physical property model. The first term enforces

model compactness through a weighted p-norm applied to the transformed model parameters, while the second term imposes smoothness constraints on the spatial variability of the model in the x, y, and z directions using a weighted q-norm. In this formulation, $\mathbf{R_s}$ and $\mathbf{R_r}$ denote regularization transform operators acting on the model and its spatial derivatives, respectively. The operator $\mathbf{D}_r$ represents the discrete first-order derivative of the model (m) along the spatial direction $r \in \{x, y, z\}$, thereby capturing the model's spatial variability in each direction. The weighting matrices $\mathbf{W_s}$ and $\mathbf{W_r}$, together with the scaling operators $\mathbf{V_s}$ and $\mathbf{V_r}$, control the relative contribution of the model parameters and their spatial derivatives. The regularization parameters α_s and α_r balance the influence of the sparsity-promoting and smoothness-promoting terms, enabling flexible control over model compactness and spatial continuity, and ultimately leading to geologically consistent and stable inversion results [20].

In this study, the inversion is carried out using a projected Gauss–Newton conjugate gradient (GNCG) optimization scheme. To ensure stability and robustness of the recovered model, multiple stopping criteria are imposed. The inversion is terminated when the data misfit reaches the level consistent with the assumed noise in the observations. Within the iterative reweighted least squares (IRLS) framework, convergence is further assessed based on the relative change in the objective function between successive iterations. Specifically, the IRLS process is stopped when this relative change falls below 10^{-4}or when a maximum of 30 iterations is reached, whichever occurs first, while an additional global iteration limit is also enforced as a safeguard against excessive computation. In addition, a sensitivity-based weighting strategy is adopted to improve the balance between well-resolved and poorly resolved regions of the model. This weighting scheme accounts for the spatial distribution of sensitivity in the forward operator, thereby enhancing the stability of the inversion and reducing artifacts in areas with low data coverage. Collectively, these criteria and weighting strategy ensure a controlled inversion process that avoids overfitting while maintaining consistency with the noise characteristics and resolving power of the data.

3 Forward Modeling and Inversion Results

To evaluate the performance of the proposed inversion framework, a synthetic full-tensor gravity-gradient model was designed and inverted under controlled conditions. The subsurface model extends from a depth of 800 m to 6000 m, while the horizontal dimensions in both the east–west and north–south directions range from 5000 m to 7000 m. To simulate realistic acquisition conditions, Gaussian noise with an amplitude of 1% was independently added to each tensor component prior to inversion. The inversion was performed using a mixed-norm regularization approach with ℓ_{01}-norm, aiming to recover compact and geologically focused density structures. The maximum number of inversion iterations was set to 30 in order to ensure convergence while maintaining computational efficiency. Furthermore, upper and lower bounds of +0.6 g/cm^3 and -0.6 g/cm^3 were imposed on the density model to constrain the inversion results within physically reasonable limits. Figure 1 illustrates the synthetic forward model used in this study. Figure 2 presents the inversion results obtained from the individual components of the full gravity gradient tensor, while Figure 3 shows the observed data, predicted responses, and corresponding residuals

(data misfit) for each tensor component. These results provide a comprehensive evaluation of the inversion performance and the resolving capability of the different FTG components.

To evaluate the performance of the proposed inversion framework, a synthetic full-tensor gravity-gradient model was designed and inverted under controlled conditions. The subsurface model extends from a depth of 800 m to 6000 m, while the horizontal dimensions in both the east–west and north–south directions range from 5000 m to 7000 m. To simulate realistic acquisition conditions, Gaussian noise with an amplitude of 1% was independently added to each gravity tensor component prior to inversion. In addition, a synthetic full-tensor magnetic dataset was generated for the same model geometry. For the magnetic data, Gaussian noise with an amplitude of 2% was added to each tensor component. The inversion of gravity data was carried out using a mixed-norm regularization approach with an ℓ_{01}-norm formulation, with density bounds of +0.6 g/cm^3 and −0.6 g/cm^3 imposed to ensure physically plausible solutions. For the magnetic inversion, susceptibility bounds of 0.3 and 0 SI were applied. The maximum number of inversion iterations was set to 30 in order to ensure convergence while maintaining computational efficiency. Figure 1 illustrates the synthetic forward models used in this study. Figure 2 presents the inversion results obtained from the individual components of the full gravity gradient tensor, while Figure 3 shows the observed data, predicted responses, and corresponding residuals (data misfit) for each gravity tensor component. Similarly, Figure 4 presents the inversion results for the full-tensor magnetic data, and Figure 5 displays the observed, predicted, and residual magnetic responses. These results provide a comprehensive evaluation of the performance of the proposed framework and demonstrate the resolving capabilities of both gravity and magnetic full-tensor components.

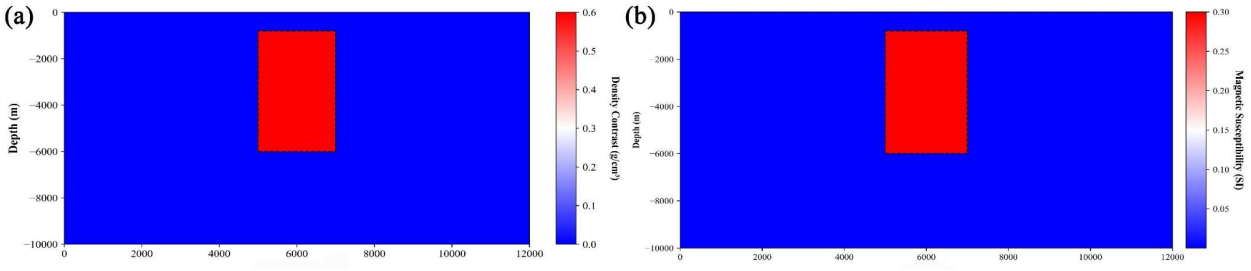

Figure 1: 2D cross-sections of the synthetic forward models used in this study for gravity and magnetic forward modelling, representing the subsurface density and susceptibility distributions. The models are identical in both the east–west (E–W) and north–south (N–S) directions. (a) Gravity forward model. (b) Magnetic forward model.

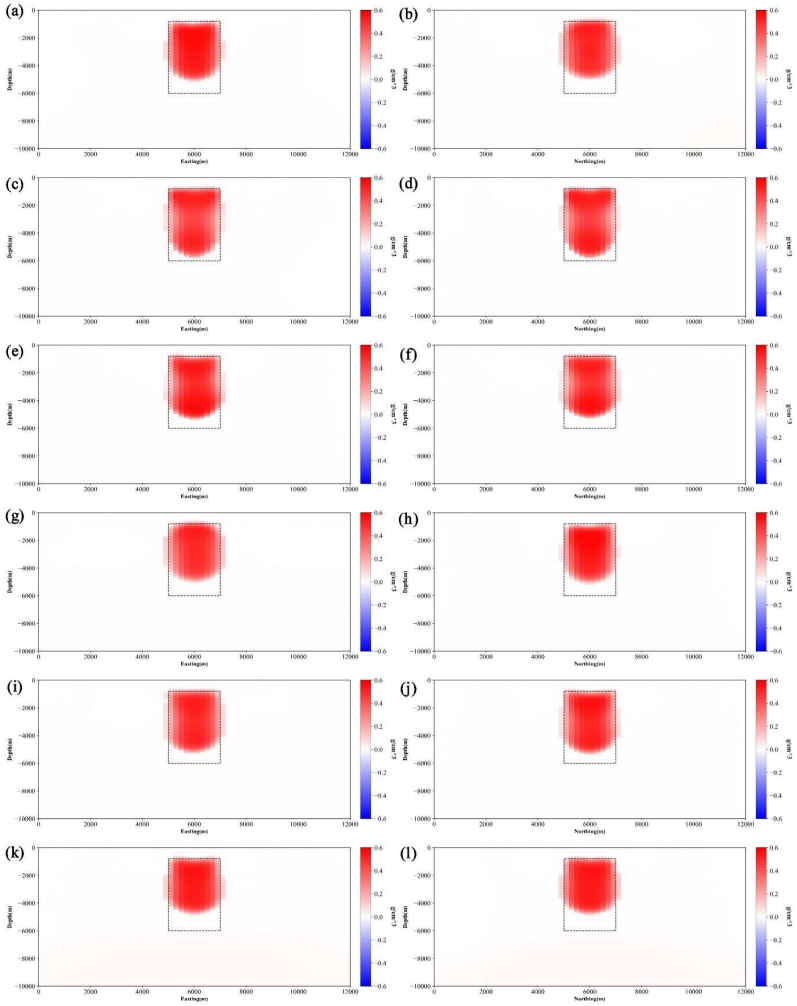

Figure 2: Inversion results of the full-tensor gravity-gradient components generated from the synthetic forward model along the east–west (E–W) and north–south (N–S) directions. Panels (a) and (b) show the g_{xx} component, panels (c) and (d) show the g_{xy} component, panels (e) and (f) show the g_{xz} component, panels (g) and (h) show the g_{yy} component, panels (i) and (j) show the g_{yz} component, and panels (k) and (l) show the g_{zz} component for the E–W and N–S profiles, respectively.

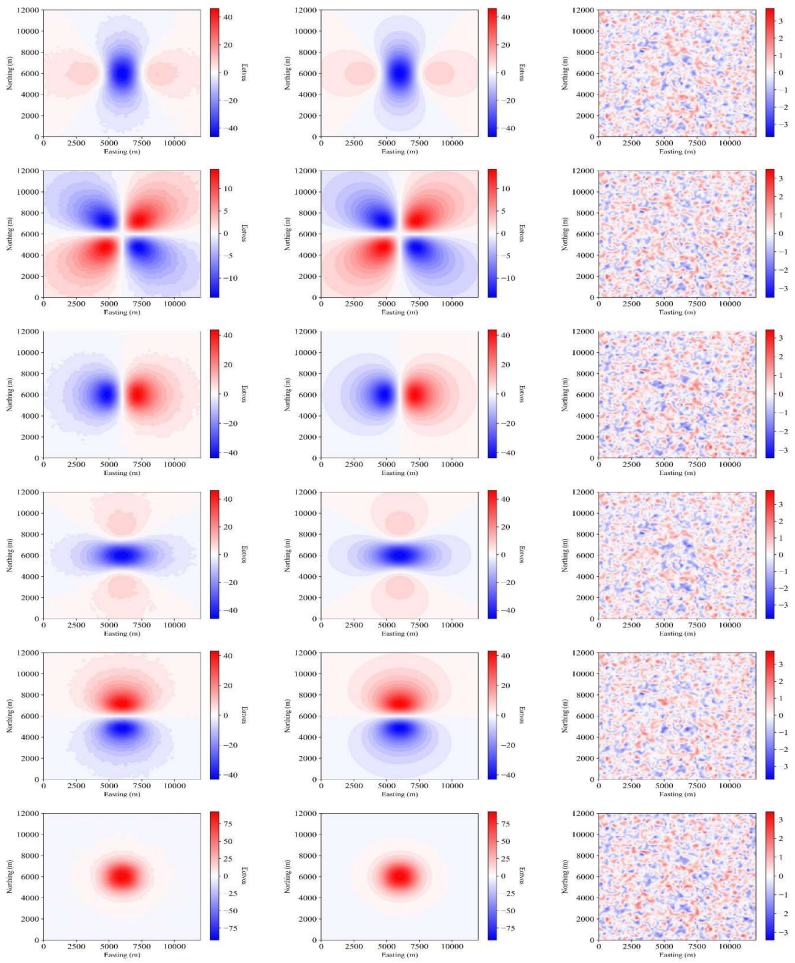

Figure 3: Comparison between the observed, predicted, and residual full-tensor gravity-gradient data for all tensor components. The first, second, and third columns represent the observed data, predicted data, and data residuals (misfit), respectively. Each row corresponds to a different tensor component: g_{xx}, g_{xy}, g_{xz}, g_{yy}, g_{yz}, and g_{zz}, respectively. The residual maps indicate the quality of the inversion and the agreement between the observed and recovered responses.

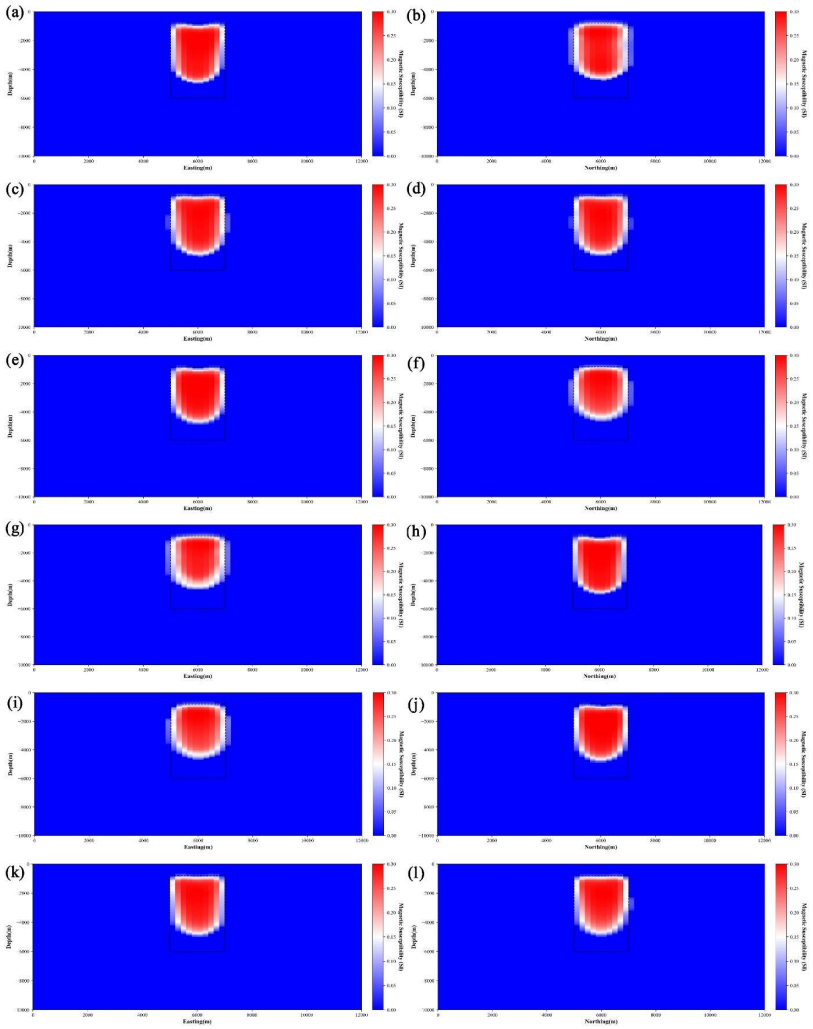

Figure 4: Inversion results of the full-tensor magnetic gradient components generated from the synthetic forward model along the east–west (E–W) and north–south (N–S) directions. Panels (a) and (b) show the b_{xx} component, panels (c) and (d) show the b_{xy} component, panels (e) and (f) show the b_{xz} component, panels (g) and (h) show the b_{yy}, component, panels (i) and (j) show the b_{yz}, component, and panels (k) and (l) show the b_{zz} component for the E–W and N–S profiles, respectively.

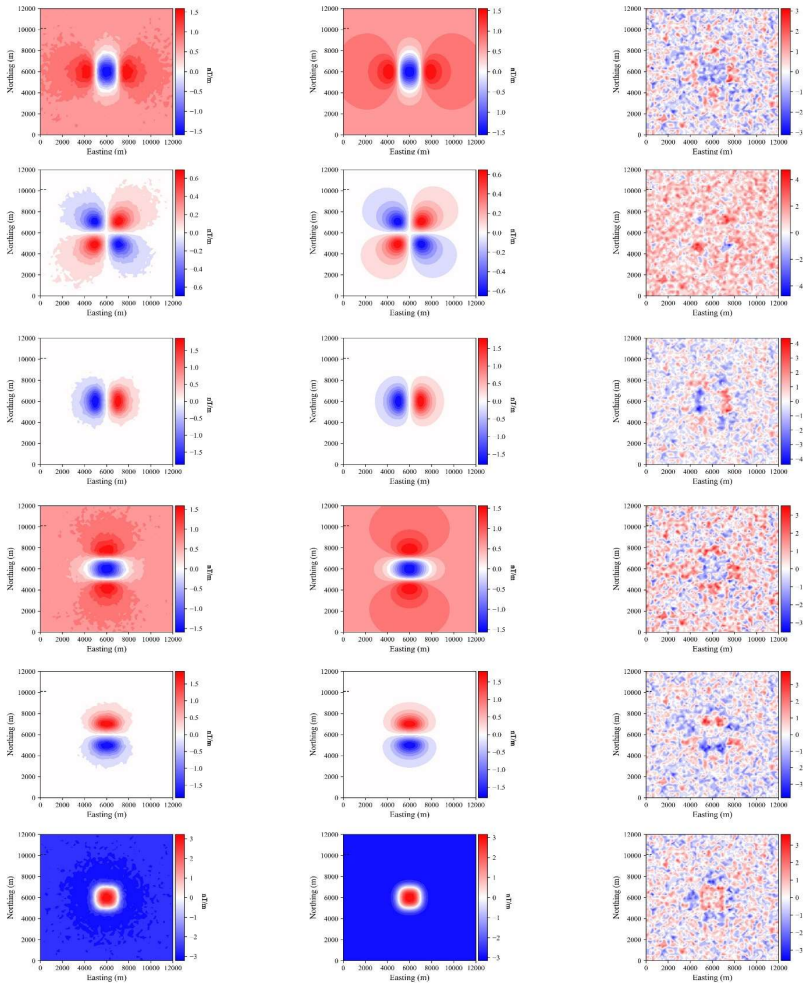

Figure 5: Comparison between the observed, predicted, and residual full-tensor magnetic data for all tensor components. The first, second, and third columns represent the observed data, predicted data, and data residuals (misfit), respectively. Each row corresponds to a different component of the magnetic gradient tensor: b_{xx}, b_{xy}, b_{xz}, b_{yy}, b_{yz}, and b_{zz}, respectively. The residual maps reflect the quality of the inversion and the level of agreement between the observed and reconstructed full-tensor magnetic responses.

4 Conclusions

In this study, a comprehensive framework for forward modelling and inversion of full-tensor gravity-gradient and full-tensor magnetic data using a mixed-norm regularization approach was developed and evaluated. The forward modelling results demonstrate that the use of the complete set of gravity and magnetic tensor components provides richer and more complementary information about subsurface physical property variations compared to single-component formulations, leading to a more reliable representation of complex geological structures. The inversion results further indicate that the proposed mixed-norm formulation is capable of simultaneously recovering both the large-scale continuity and the sharp boundaries of subsurface features for density and susceptibility distributions. The inversion is performed using a projected Gauss–Newton conjugate gradient (GNCG) algorithm combined with an iterative reweighted least squares (IRLS) scheme, ensuring stable convergence of the inversion process for both datasets,

even in the presence of 1% Gaussian noise in gravity and 2% Gaussian noise in magnetic data. In addition, a sensitivity-based weighting strategy is incorporated into the inversion framework, which improves the balance between well-resolved and poorly resolved regions of the model and enhances the robustness of the recovered solutions. The inclusion of physical property bounds further contributes to stabilizing the inversion and reducing non-physical artifacts. A comparative analysis of the different tensor components in both gravity and magnetic datasets reveals that each component exhibits distinct sensitivity to subsurface structures, and their joint use substantially improves the spatial resolution and interpretability of the inversion results. Overall, the results demonstrate that the integration of full-tensor gravity and full-tensor magnetic forward modelling with mixed-norm inversion, together with sensitivity-based weighting, provides a robust and effective framework for high-resolution subsurface imaging, particularly in geologically complex environments, and holds strong potential for integrated geophysical exploration.

Acknowledgments

We extend our heartfelt gratitude to the Faculty of Mining Engineering at the University of Tehran for their invaluable support in the execution of this research.

References

[1] R.J. Blakely, *Potential Theory in Gravity and Magnetic Applications*. Cambridge University Press, 1996.

[2] W.J. Hinze, R.R. von Frese, and A.H. Saad, *Gravity and Magnetic Exploration: Principles, Practices, and Applications*. Cambridge University Press, 2013.

[3] Y. Li and D.W. Oldenburg, "3-D inversion of magnetic data," *Geophysics*, vol. 61, no. 2, pp. 394–408, 1996.

[4] W.M. Telford, L.P. Geldart, and R.E. Sheriff, *Applied Geophysics*. Cambridge University Press, 1990.

[5] Y. Li and D.W. Oldenburg, "3-D inversion of gravity data," *Geophysics*, vol. 63, no. 1, pp. 109–119, 1998.

[6] M.N. Nabighian et al., "75th Anniversary: The historical development of the magnetic method in exploration," *Geophysics*, vol. 70, no. 6, pp. 33ND–61ND, 2005.

[7] Y. Feng et al., "An intriguing property of geophysical inversion," in *Proc. ICML*, 2022.

[8] C.-W. Guo et al., "Three-directional analytic signal analysis and interpretation of magnetic gradient tensor," *Appl. Geophys.*, vol. 17, no. 2, pp. 285–296, 2020.

[9] M.H. Dransfield, "Airborne gravity gradiometry," 1994.

[10] M. Geng et al., "3-D joint inversion of airborne gravity gradiometry and magnetic data using a probabilistic method," *Geophys. J. Int.*, vol. 223, no. 1, pp. 301–322, 2020.

[11] X. Tu and M.S. Zhdanov, "Joint focusing inversion of marine controlled-source electromagnetic and full tensor gravity gradiometry data," *Geophysics*, vol. 87, no. 5, pp. K35–K47, 2022.

[12] L. Zhang et al., "Deep learning for 3-D inversion of gravity data," *IEEE Trans. Geosci. Remote Sens.*, vol. 60, pp. 1–18, 2021.

[13] L.B. Pedersen and T.M. Rasmussen, “The gradient tensor of potential field anomalies,” *Geophysics*, vol. 55, no. 12, pp. 1558–1566, 1990.

[14] D.A. Clark, “Corrigendum: New methods for interpretation of magnetic vector and gradient tensor data I,” *Explor. Geophys.*, vol. 45, no. 4, pp. 267–282, 2014.

[15] Z.-L. Hou et al., “Full tensor gravity gradiometry data inversion: performance analysis of parallel computing algorithms,” *Appl. Geophys.*, vol. 12, no. 3, pp. 292–302, 2015.

[16] C.A. Murphy, “The Air-FTG airborne gravity gradiometer system,” in *Airborne Gravity*, pp. 7–14, 2004.

[17] A.N. Tikhonov and V. Arsenin, *Solutions of Ill-Posed Problems*. 1977.

[18] W. Menke, *Geophysical Data Analysis: Discrete Inverse Theory*. Academic Press, 2018.

[19] P.C. Hansen, *Discrete Inverse Problems: Insight and Algorithms*. SIAM, 2010.

[20] D. Fournier, *Advanced Potential Field Data Inversion with Lp-Norm Regularization*. University of British Columbia, 2019.

[21] D. Fournier, D.W. Oldenburg, and K. Davis, “Robust and flexible mixed-norm inversion,” in *SEG Int. Exposition and Annual Meeting*, 2016.

[22] R. Cockett et al., “SimPEG: An open-source framework for simulation and gradient-based parameter estimation in geophysical applications,” *Comput. Geosci.*, vol. 85, pp. 142–154, 2015.

[23] M.S. Zhdanov, *Inverse Theory and Applications in Geophysics*, vol. 36. Elsevier, 2015.

[24] D. Nagy, “The gravitational attraction of a right rectangular prism,” *Geophysics*, vol. 31, no. 2, pp. 362–371, 1966.

[25] J. Sun and X. Wei, “Recovering sparse models in 3D potential-field inversion using mixed Lp norm regularization,” *Geophys. Prospect.*, vol. 69, no. 4, pp. 901–910, 2021.

[26] D. Fournier and D.W. Oldenburg, “Inversion using spatially variable mixed ℓp norms,” *Geophys. J. Int.*, vol. 218, no. 1, pp. 268–282, 2019.

[27] V. Sharma, “Rapid computation of magnetic anomalies and demagnetization effects caused by bodies of arbitrary shape,” *Pure Appl. Geophys.*, vol. 64, no. 1, pp. 89–109, 1966.